Available online at www.sciencedirect.com
SCIENCE DIRECT®
Planetary and Space Science 53 (2005) 945–957
Planetary and Space Science
www.elsevier.com/locate/pss

Reconstruction of ion and electron density profiles from space-based measurements of the upper electron content

S.M. Stankov[a,*], N. Jakowski[a], S. Heise[b]

[a]German Aerospace Centre (DLR), Institute of Communications and Navigation, D-17235 Neustrelitz, Germany
[b]GeoForschungsZentrum Potsdam (GFZ), D-14473 Potsdam, Germany

Received 10 July 2003; received in revised form 2 March 2005; accepted 15 April 2005

Abstract

Presented is a new method for retrieving the topside electron density distribution from space-based observations of the total electron content. By assuming an adequate topside density distribution, the profile reconstruction technique utilizes ionosonde and oxygen–hydrogen ion transition level measurements for uniquely determining the unknown ion scale heights and the corresponding ion and electron density profiles. The method is tested on actual measurements from the CHAMP satellite. Important applications are envisaged, such as developing and evaluating empirical and theoretical ionosphere–plasmasphere models.

Keywords: Electron density profile; Reconstruction method; Low-earth-orbiting satellite

1. Introduction

Reliable information on the top-side ionospheric and plasmaspheric density distribution is required in various practical activities such as the estimation and correction of Global Navigation Satellite System (GNSS) propagation delays, investigation of space-weather effects on telecommunications, etc. If available in real-time, the top-side electron profiles can be a valuable input to the space-weather forecasting (Huang and Reinisch, 2001). Until recently, such reliable information was difficult to obtain. Older techniques, such as the vertical incidence sounding, provided reliable but bottom-side profiles only. Significant progress has been made with the digital ionosondes (Reinisch et al., 2001) and automated procedures have been developed for electron density profiling (Reinisch and Huang, 1982; Huang and Reinisch, 1982; Reinisch and Huang, 1983). However, the topside profiling needs further improvement. Other techniques, such as the incoherent scatter probing, top-side sounding from satellites, in situ rocket and satellite observations, are available but can be expensive or can provide observations limited in space and/or time.

The Total Electron Content (TEC) measurements (Leitinger, 1996a) gave a new impetus to finding other ways to gain valuable information on the top-side ionosphere ionization, and particularly for developing a powerful imaging technique—the ionosphere tomography (Austen et al., 1988; Leitinger, 1996b). The Global Positioning System (GPS) and the ground-based TEC measurements using GPS have also become well-established tools for monitoring the outer ionosphere (Coco, 1991; Jakowski, 1996; Davies and Hartmann, 1997). These measurements can be used successfully for deduction of the vertical ion and electron density profiles. In an earlier publication (Stankov and Muhtarov, 2001) reported was a new method developed for deducing the electron profiles from ground-based measurements of TEC and formulated by using the Sech-squared profiler (Rawer, 1988; Davies, 1990). It has been tested with real data (Stankov et al., 2002) and the results were promising. A detailed analysis (Stankov,

*Corresponding author. Tel.: +49 3981 480 113; fax: +49 3981 480 123.
E-mail address: stanimir.stankov@dlr.de (S.M. Stankov).

0032-0633/$ - see front matter © 2005 Elsevier Ltd. All rights reserved.
doi:10.1016/j.pss.2005.04.008

2002c) of the reconstruction behaviour of various analytical ionospheric models, namely the Sech-squared, Chapman, and Exponential profilers (Davies, 1990, 1996), showed that the Exponential profiler is much better suited for day-time density reconstruction than the original scheme with the Sech-squared profiler.

Recent developments in the GPS receiver technology allowed for signal receivers to be placed onboard Low-altitude earth-orbiting (LEO) satellites. This opportunity revived the occultation technique (Fjeldbo et al., 1971) to be applied successfully for deducing electron density distribution (Jakowski et al., 2002) and atmospheric parameters such as temperature, pressure and water vapour (Gurvich and Krasilnikova, 1990; Hoeg et al., 1995). LEO satellites can deliver the electron content above the height of the satellite, the so-called over-satellite electron content (OSEC). Numerically, OSEC integrates the vertical electron density from the height of the receiving satellite, h_s ($h_s > h_m F_2$), up to the ceiling height, h_c ($h_c \gg h_s$), and it will be denoted also with TEC(h_s, h_c) or *s*TEC.

The purpose of this paper is to present a new method for the reconstruction of the vertical electron density profile from the vertical over-satellite TEC measured by a LEO satellite. The difference of the proposed method from other existing density reconstruction techniques is that it employs two additional types of measurements—ionosonde observations and empirical values of the O^+–H^+ ion transition height (upper transition level, UTL), i.e. the height where the H^+ density equals the O^+ density. In this way, information from independent sources is utilized, which is expected to improve the quality of reconstruction (Stankov et al., 2003a) and eventually to be used for operational monitoring (Stankov et al., 2003b). However, the reconstruction technique using ground based TEC measurements is not applicable to LEO satellite measurements due to the existing gap between bottom-side measurements (i.e. below the peak density height $h_m F_2$) and measurements over the LEO satellite height (Fig. 1); it should be noted that, in some cases, the gap can extend up to several hundred kilometers. Therefore, a separate treatment of the space-based reconstruction is required.

The paper is structured in the following way. First, the reconstruction method is detailed. Second, the input data required for the method are presented. Next, some exemplary calculations are made with CHAMP data. Finally, comparison is made between results of this reconstruction and other methods and models.

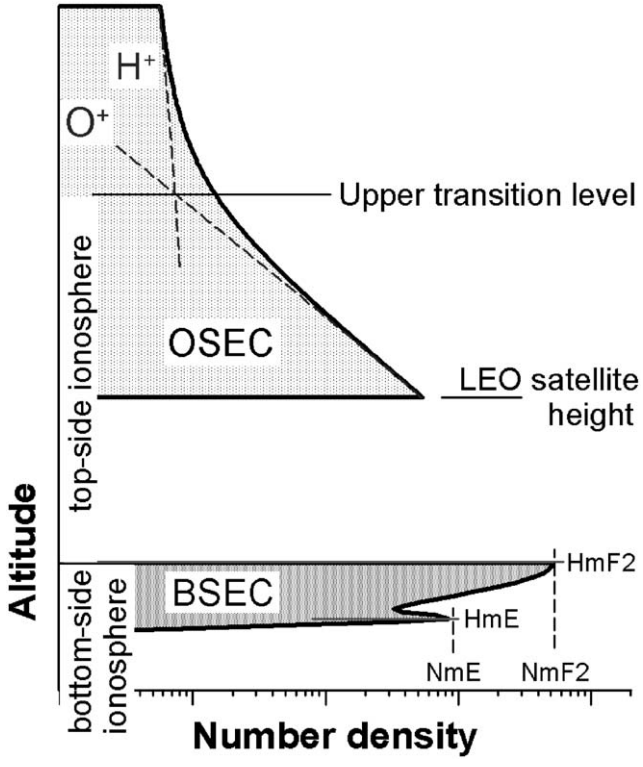

Fig. 1. A schematic view of the topside ion and electron density distribution.

2. Reconstruction method

The method is developed for determination of the upper electron profile, i.e. above $h_m F_2$. For this purpose, the profile is presented as a sum of its major constituents—the oxygen and hydrogen ion density profiles. Because of the known presence in the upper atmosphere of atomic hydrogen and because of the charge-exchange reaction between hydrogen atoms and oxygen ions, the presence of the H^+ ions in the topside F_2 layer cannot be neglected. As a result, the presence in the diffusion problem of two ion species, especially with such different atomic weights, greatly complicates it. Further, the individual ion density distributions are approximated by the hyperbolic secant function in the following manner:

$$N_i(h) = N_i(h_m)\,\mathrm{sech}^2\left(\frac{h-h_m}{2H_i}\right), \tag{1}$$

where $N_i(h)$ is the oxygen or hydrogen ion density at height h, H_i is the ion scale height, and sech(.) is the secant hyperbolic function. The following 'reconstruction' formula is proposed for calculation of the upper electron density profile:

$$N_e(h) = N_{O+}(h_m)\,\mathrm{sech}^2\left(\frac{h-h_m}{2H_{O+}}\right) + N_{H+}(h_m)\,\mathrm{sech}^2\left(\frac{h-h_m}{2H_{H+}}\right), \quad h > h_m, \tag{2}$$

where $N_e(h)$ is the electron density at height h, H_{O+} is the O^+ scale height, H_{H+} is the H^+ scale height,

$N_{O+}(h_m)$ and $N_{H+}(h_m)$ are the O^+ and H^+ densities at the height h_m of the F_2-layer maximum electron density.

The necessity of reconstructing the density distribution in the vertical direction and the fact that the plasma transport is predominantly along the geomagnetic field line required the use of a 'vertical' corrector (Fig. 2). The sole purpose of this correction factor is to 'map' the scale height along the magnetic field line onto the vertical axis, which in effect re-distributes the plasma density in height direction. Under the assumption that the ionosphere and plasmasphere are isotropic, the scale heights of O^+ and H^+ along the magnetic field lines will have a ratio 1:16 following the definition of scale height. Also, the H^+ is supposed to decrease exponentially above the level of h_mF_2 which is true but for altitudes above the O^+–H^+ transition height. To obtain the vertical density distribution (see also Section 6.2), the conversion $dh = \sin I\, ds$ is applied, where dh is the differential element along the vertical, ds is the differential element along the field line, and I is the inclination. If the displacement of the geographic and geomagnetic poles is ignored then $dh = \sin[\arctan(2.\tan\varphi)]\, ds$, where φ is the dip latitude. Thus, by introducing $\xi = \sin[\arctan(2.\tan\varphi)]$, the reconstruction formula will read:

$$N_e(h) = N_{O+}(h_m)\,\mathrm{sech}^2\left(\frac{h-h_m}{2H_{O+}}\right) + N_{H+}(h_m)\,\mathrm{sech}^2\left(\frac{h-h_m}{32\xi H_{O+}}\right), \quad h > h_m. \tag{3}$$

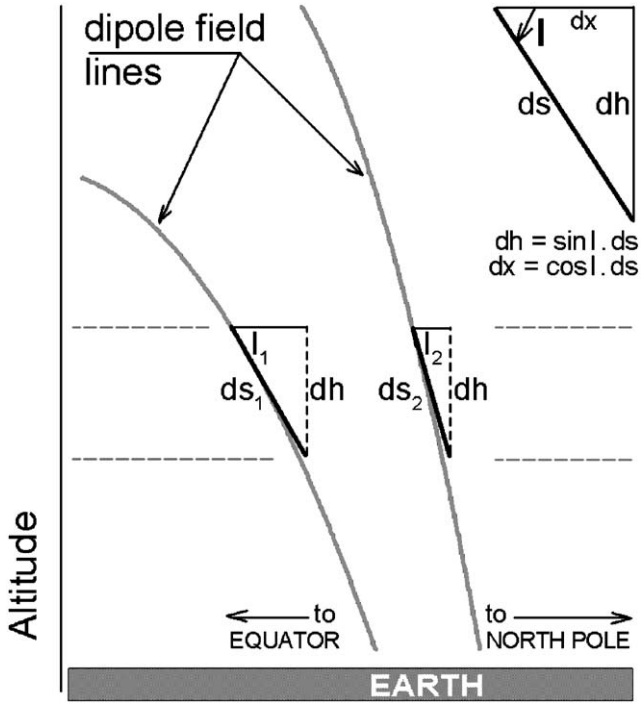

Fig. 2. The use of a vertical corrector for 'mapping' the scale height along the magnetic field line onto the vertical axis.

There are three unknown variables in the proposed formula—the oxygen and hydrogen ion densities at the peak height, i.e. $N_{O+}(h_m)$ and $N_{H+}(h_m)$, and the oxygen ion scale height H_{O+}. These unknowns are determined in the following way.

The over-satellite electron content is the difference between the topside electron content (above h_m) and the electron content enclosed in-between the heights h_m and h_s, i.e.:

$$sTEC = TEC(h_s;h_c) = TEC(h_m;h_c) - TEC(h_m;h_s) = \int_{hm}^{hc} N_e(h)\,dh - \int_{hm}^{hs} N_e(h)\,dh. \tag{4}$$

Both integrals are solved similarly (Stankov, 2002b) and, for a scale height H, the result is

$$\int_{hm}^{hs} N(h)\,dh = 2HN(h_m)\frac{1-\exp\left(\frac{h_m-h_s}{H}\right)}{1+\exp\left(\frac{h_m-h_s}{H}\right)}, \tag{5}$$

$$\int_{hm}^{hc} N(h)\,dh = 2HN(h_m). \tag{6}$$

Further, after integrating $N_e(h)$ using the 'reconstruction' formula, and considering the above integral solutions, it follows that

$$TEC(h_m,h_c) = 32\xi H_{O+}N_m + 2(1-16\xi)H_{O+}N_{O+}(h_m), \tag{7}$$

$$TEC(h_m,h_s) = 32\xi X_{H+}H_{O+}N_m + 2(X_{O+}-16\xi X_{H+}) \times H_{O+}N_{O+}(h_m), \tag{8}$$

$$X_{O+} = \left[1-\exp\left(\frac{h_m-h_s}{H_{O+}}\right)\right] \Big/ \left[1+\exp\left(\frac{h_m-h_s}{H_{O+}}\right)\right], \tag{9}$$

$$X_{H+} = \left[1-\exp\left(\frac{h_m-h_s}{16\xi H_{O+}}\right)\right] \Big/ \left[1+\exp\left(\frac{h_m-h_s}{16\xi H_{O+}}\right)\right]. \tag{10}$$

Hence, the over-satellite electron content is

$$sTEC = 4Y_{O+}H_{O+}N_{O+}(h_m) + 4Y_{H+}H_{H+}N_{H+}(h_m) = 64\xi Y_{H+}H_{O+}N_m + 4[Y_{O+}-16\xi Y_{H+}] \times H_{O+}N_{O+}(h_m). \tag{11}$$

$$Y_{O+} = \exp\left(\frac{h_m-h_s}{H_{O+}}\right) \Big/ \left[1+\exp\left(\frac{h_m-h_s}{H_{O+}}\right)\right]. \tag{12}$$

$$Y_{H+} = \exp\left(\frac{h_m-h_s}{16\xi H_{O+}}\right) \Big/ \left[1+\exp\left(\frac{h_m-h_s}{16\xi H_{O+}}\right)\right]. \tag{13}$$

Using the principle of quasi-neutrality and Eq. 11, the F_2 peak ion densities can be expressed as:

$$N_{O+}(h_m) = (sTEC - 64\xi Y_{H+} H_{O+} N_m) / [4(Y_{O+} - 16\xi Y_{H+}) H_{O+}], \quad (14)$$

$$N_{H+}(h_m) = (4 Y_{O+} H_{O+} N_m - sTEC) / [4(Y_{O+} - 16\xi Y_{H+}) H_{O+}], \quad (15)$$

Finally, after a series of transformations (Stankov, 2002b), the following transcendental equation is constructed for obtaining the unknown O^+ scale height:

$$\frac{sTEC - 64\xi Y_{H+} H_{O+} N_m}{4(Y_{O+} - 16\xi Y_{H+}) H_{O+} N_m} \left\{ \operatorname{sech}^2\left(\frac{h_{tr} - h_m}{2H_{O+}}\right) + \operatorname{sech}^2\left(\frac{h_{tr} - h_m}{32\xi H_{O+}}\right) \right\} = \operatorname{sech}^2\left(\frac{h_{tr} - h_m}{32\xi H_{O+}}\right). \quad (16)$$

The unknown oxygen ion scale height is obtained after numerically solving the above transcendental equation (16). Once the O^+ scale height is found, it is easy to compute the ion densities $N_{O+}(h_m)$ and $N_{H+}(h_m)$ using expressions (14) and (15). The upper electron density profile is then recovered by using the reconstruction formula (3).

The described technique is not restricted to the use of one particular profiler. A study of various analytical ionospheric models (Stankov, 2002c) shows that others can be adopted as well, for example the Exponential model:

$$N(h) = N(h_m) \exp\left(-\frac{h - h_m}{H}\right). \quad (17)$$

In this case the reconstruction formula is

$$N_e(h) = N_{O+}(h_m) \exp\left(\frac{h - h_m}{2H_{O+}}\right) + N_{H+}(h_m) \exp\left(\frac{h - h_m}{32\xi H_{O+}}\right), \quad h > h_m \quad (18)$$

and most of the calculations are carried out in a similar way as for the Sech-squared layer. This time, the O^+ and H^+ densities at h_m are expressed in the form:

$$N_{O+}(h_m) = \frac{sTEC - 16\xi Y_{H+} N_m}{(Y_{O+} - 16 Y_{H+}) H_{O+}}, \quad (19)$$

$$N_{H+}(h_m) = \frac{Y_{O+} H_{O+} N_m - sTEC}{(Y_{O+} - 16 Y_{H+}) H_{O+}}, \quad (20)$$

$$Y_{O+} = \exp\left(\frac{h_m - h_s}{H_{O+}}\right), \quad (21)$$

$$Y_{H+} = \exp\left(\frac{h_m - h_s}{16\xi H_{O+}}\right) \quad (22)$$

and the transcendental equation (O^+ scale height is the variable) acquires the following form:

$$\frac{sTEC - 16\xi Y_{H+} H_{O+} N_m}{(Y_{O+} - 16\xi Y_{H+}) H_{O+} N_m} \left\{ \exp\left(\frac{h_m - h_{tr}}{H_{O+}}\right) + \exp\left(\frac{h_m - h_{tr}}{16\xi H_{O+}}\right) \right\} = \exp\left(\frac{h_m - h_{tr}}{16\xi H_{O+}}\right). \quad (23)$$

Now, the unknown oxygen ion scale height is obtained after numerically solving the above transcendental equation (23). Once the O^+ scale height is found, it is used for computing the ion densities $N_{O+}(h_m)$ and $N_{H+}(h_m)$ using expressions (19) and (20). Finally, the upper electron density profile is deduced with the help of reconstruction formula (18).

3. Space-based observations of TEC

LEO satellites performing dual frequency GPS navigation measurements are convenient instruments for obtaining information on the physical processes taking place in the topside ionosphere and the plasmasphere. There are currently several LEO satellites in operation, for example Challenging Minisatellite Payload (CHAMP), Satelite de Aplicaciones Cientificas-C (SAC-C), and Gravity Recovery And Climate Experiment (GRACE). In this study we used topside electron density reconstructions based on GPS navigation data from CHAMP.

3.1. CHAMP satellite mission

The German geo-research satellite CHAMP was launched on 15 July, 2000 into a circular and polar orbit at an 87° inclination and at an initial altitude of 454 km (Reigber et al., 2003). One of the reasons for choosing a circular and polar orbit is the benefit of acquiring a homogeneous and complete global coverage of the Earth's space environment. An advantage of an 87° orbit vs. a dawn–dusk sun-synchronous orbit is the local time variation of the satellite's ground track which is essential for the scientific experiments. It enables the separation of periodic phenomena constituents such as tides and day–night variations. CHAMP is equipped with new generation receivers ("Black Jack") having novel capabilities like "enhanced codeless" tracking (ability to track encrypted GPS signals), higher signal-to-noise ratio, and lower tracking in the atmosphere.

3.2. GPS TEC data acquisition

The TEC calculation is based on a newly developed model-assisted technique for reconstruction of the three-dimensional (3D) electron density structure above the

CHAMP orbit from GPS observations. Two types of input are required for the retrieval algorithm: GPS navigation measurements from CHAMP (0.1 Hz) and orbit data for CHAMP and the involved GPS satellites. The data processing and retrieval method (Heise et al., 2002) consists of the following main parts—GPS data pre-processing, calibration of link related TEC, and assimilation of calibrated TEC. During the pre-processing stage, detected outliers are being removed and cycle slips corrected. The ionospheric combination of GPS pseudoranges and carrier phases is used to derive the TEC value. TEC is consistently calibrated for receiver and satellite differential group delay biases. The calibration of numerous link-related TEC values for instrumental biases is performed with the help of the Parameterized Ionospheric Model (PIM) (Daniell et al., 1995). Considering that GPS differential code biases are reliably estimated by GPS processing centres, the calibration procedure is focused on the estimation of the CHAMP receiver bias only. Results show that the estimated bias is quite stable—variations not exceeding 1 TECU ($1\ \mathrm{TECU} = 10^{16}\ \mathrm{m}^{-2}$). The final part, the assimilation of calibrated but link-related TEC data into the PIM model, is used to deduce the 3D electron density distribution using a global 3D voxel structure. It involves an iterative process that modifies the electron densities inside the voxels crossed by CHAMP-GPS radio links until the integrated electron density along the radio link equals the corresponding link-related TEC value. Finally, OSEC is derived by vertical reintegration of the 3D assimilation results.

4. Ionosonde observations

Previous TEC studies suggest that the bottom-side profile (below the F-layer peak electron density height, h_mF_2) should be more precisely modeled, and if possible, connected to measurements of the ground vertical ionospheric soundings. In this part, a reliable and flexible way of profiling the bottom-side electron density distribution will be described. Required ionosonde data are the F_2-layer critical frequency (f_oF_2), the propagation factor ($M_{3000}F_2$), and the E-layer critical frequency (f_oE).

The vertical electron density distribution below h_mF_2 is calculated with the Epstein layer:

$$N_e(h) = N_e(h_m)\ \mathrm{sech}^2\left(\frac{h-h_m}{B_{bot}}\right), \tag{1}$$

where $N_e(h)$ is the electron density, B_{bot} is the bottom-side thickness, and

$$\mathrm{sech}(h) = 1/\cosh(h), \quad \cosh(h) = 0.5(\exp(h)+\exp(-h)). \tag{2}$$

The F_2-layer peak height is estimated using the expression (Dudeney, 1983):

$$h_mF_2 = -176 + 1470\frac{M_{3000}F_2\left\{\left[0.0196(M_{3000}F_2)^2+1\right]/\left[1.296(M_{3000}F_2)^2-1\right]\right\}^{1/2}}{M_{3000}F_2 - 0.012 + 0.253/(f_oF_2/f_oE - 1.215)}. \tag{3}$$

The bottom-side thickness, B_{bot}, is calculated by (Di Giovanni and Radicella, 1990): $B_{bot} = 0.385N_mF_2(\mathrm{d}N/\mathrm{d}h)^{-1}_{max}$, where $(\mathrm{d}N/\mathrm{d}h)_{max}$ is the value of the gradient of $N_e(h)$ at the base of the F_2 layer, and it is determined by the following formula:

$$\begin{aligned}(\mathrm{d}N/\mathrm{d}h)_{max}[10^9\ \mathrm{m}^{-3}\ \mathrm{km}^{-1}] &= \exp\{-3.467 + 0.857 \\ &\times \ln(f_oF_2[\mathrm{MHz}])^2 + 2.02\ln(M_{3000}F_2)\}.\end{aligned} \tag{4}$$

When F_2 and E layers are both present in the ionograms, the bottom-side profile is constructed as a sum of two identical Epstein layers (Rawer, 1988):

$$\begin{aligned}N(h) = &\{4N_m\exp[(h-h_m)/B_{bot}]\} \\ &/\{1+\exp[(h-h_m)/B_{bot}]\}^2,\end{aligned} \tag{5}$$

where N_m and h_m are the (F_2- or E-) layer's peak density and peak height respectively. The electron density distribution at D region heights is not modeled in detail as its contribution to the TEC is negligible. It is important to mention that alternative ways can be used to calculate parameters (for example, f_oF_2 and $M_{3000}F_2$) in case ionosonde data are missing or are unreliable, and also for real-time reconstruction.

The E-layer critical frequency, f_oE, can be calculated by the following formula (Bilitza and Rawer, 1996): $f_oE(R,\phi,\chi) = (ABCD)^{1/4}$, where R is the solar radiance, ϕ is the geographic latitude, and χ is the solar zenith angle. The components A and B express the solar activity, C—latitudinal, and D—diurnal dependence:

$$\begin{aligned}&A = 1 + 0.0094(F10.7 - 66), \\ &B = (\cos\chi_{noon})^m, && m = 1.93 + 1.92\cos\phi,\ \text{for } |\phi| < 32^\circ, \\ & && m = 0.11 - 0.49\cos\phi,\ \text{for } |\phi| \geqslant 32^\circ, \\ &C = X + Y\cos\phi, && X = 23,\ Y = 116,\ \text{for } |\phi| < 32^\circ, \\ & && X = 92,\ Y = 35,\ \text{for } |\phi| \geqslant 32^\circ, \\ &D = (\cos\chi)^p, && p = 1.31,\ \text{for } |\phi| \leqslant 12^\circ, \\ & && p = 1.20,\ \text{for } |\phi| > 12^\circ.\end{aligned}$$

The propagation factor, $M_{3000}F_2$ ($= \mathrm{MUF}/f_oF_2$), can be taken from existing empirical maps of Comite Consultatif International des Radiocommunications (CCIR) or Union Radio-Scientifique Internationale (URSI).

5. Upper ion transition level data

It is assumed that the topside ionosphere consists of two major components—oxygen and hydrogen ions and their scale heights are constant with altitude. One interesting feature of such two-ion distribution is the behaviour of these ions at and near the O^+–H^+ transition height. A sharp increase of the plasma scale height is observed at the UTL due to the following.

In the topside ionosphere region above the F_2-layer peak and below UTL the O^+ is still the predominant ion but the presence of the H^+ ions cannot be neglected. In addition, the electrons contribute to a larger scale height for ions by the establishment of an electric field resulting from a slight charge separation. The electric field is large enough so that it is a more important force than gravity for protons by a factor of 8. Consequently, the proton concentration increases with altitude and at the UTL protons become the predominant ions. Above UTL, the H^+ ions are distributed as if their atomic weight were 0.5, and oxygen ions as if their atomic weight were 15.5. The picture is further complicated by the fact that the H^+ maximum is quite often situated above the UTL. In our method, it is assumed that the peak is far below—at the height of the F_2 peak; thus, the height distribution of the hydrogen ions follows the height distribution of the atomic hydrogen and the two-slope electron profile—with a sharp increase of the scale height at the UTL—is readily obtained.

One of the main ideas behind the reconstruction technique is in the use of the O^+–H^+ transition level as a key reconstruction parameter, the anchor utilized when searching for a unique solution for the topside ion and electron density profiles. In addition to ensuring the uniqueness of solution, the use of the UTL value diminishes expected errors caused by the assumptions of constant scale height and diffusive equilibrium conditions. Here, the needed transition height is determined from an empirical model (ref. Tables 1 and 2), based mainly on satellite in situ measurements of the individual O^+ and H^+ ion densities (Kutiev et al., 1994). In this model, the transition level is approximated by a multi-variable polynomial, providing convenience when referencing the level with respect to solar activity,

Table 1
The O^+–H^+ transition height model's data base for *low solar activity* ($R = 50$): night-time (left side) and day-time (right side) values [km] for summer (top) and winter (bottom) seasons

Long	0–60	60–120	120–180	180–240	240–300	300–360	0–60	60–120	120–180	180–240	240–300	300–360
Lat	Summer: night-time						Summer: day-time					
55–65	824	824	824	824	824	824	1248	1200	1152	1152	1200	1248
45–55	765	770	765	771	775	780	1237	1189	1142	1142	1189	1237
35–45	725	730	730	735	739	739	1198	1152	1106	1106	1152	1198
25–35	714	726	732	730	727	726	1128	1085	1042	1042	1085	1128
15–25	718	714	714	712	710	714	1035	995	955	955	995	1035
5–15	749	745	745	745	745	745	988	950	893	893	950	988
0	765	765	765	765	765	765	978	940	903	903	940	978
−15–5	750	750	750	750	754	750	986	948	911	911	948	986
−25–15	724	722	720	724	728	724	1012	973	935	935	973	1012
−35–25	715	713	710	709	702	709	1043	1002	962	962	1002	1043
−45–35	730	735	739	739	725	730	1104	1061	1019	1019	1061	1104
−55–45	775	781	785	790	775	780	1136	1092	1049	1049	1092	1136
−65–55	824	824	824	824	824	824	1144	1100	1056	1056	1100	1144
Lat	Winter: night-time						Winter: day-time					
55–65	754	754	754	754	754	754	1078	1078	1100	1122	1122	1100
45–55	740	735	741	741	751	745	1070	1070	1092	1113	1113	1092
35–45	705	720	724	720	705	705	1040	1040	1061	1082	1082	1061
25–35	645	650	653	646	645	645	982	982	1002	1022	1022	1002
15–25	625	627	628	632	625	625	954	954	973	992	992	973
5–15	715	715	715	713	711	709	929	929	948	967	967	948
0	766	762	762	762	762	762	918	918	936	955	955	936
−15–5	750	748	754	754	754	752	930	930	949	968	968	949
−25–15	690	690	690	692	693	697	959	959	978	998	998	978
−35–25	635	635	635	640	643	636	994	994	1014	1034	1034	1014
−45–35	670	670	670	685	689	685	1049	1049	1070	1091	1091	1070
−55–45	725	719	716	709	715	715	1073	1073	1095	1117	1117	1095
−65–55	754	754	754	754	754	754	1078	1078	1100	1122	1122	1100

Values sorted according to geomagnetic latitude and longitude.

Table 2
The O^+–H^+ transition height model data base for increased solar activity ($R = 100$): night-time (left side) and day-time (right side) values for summer (top) and winter (bottom) seasons

Long	0–60	60–120	120–180	180–240	240–300	300–360	0–60	60–120	120–180	180–240	240–300	300–360
Lat	Summer: night-time						Summer: day-time					
55–65	1100	1100	1100	1100	1100	1100	1430	1430	1430	1430	1430	1430
45–55	922	912	902	922	942	932	1420	1420	1420	1420	1420	1420
35–45	950	940	930	940	950	950	1380	1380	1380	1380	1380	1380
25–35	1011	991	981	976	971	991	1300	1300	1300	1300	1300	1300
15–25	1040	1030	1030	1025	1020	1030	1250	1250	1250	1250	1250	1250
5–15	1049	1039	1039	1039	1039	1039	1200	1200	1200	1200	1200	1200
0	1050	1040	1040	1040	1040	1040	1150	1150	1150	1150	1150	1150
−15–5	1080	1090	1090	1090	1090	1090	1200	1200	1200	1200	1200	1200
−25–15	1050	1050	1050	1070	1070	1070	1250	1250	1250	1250	1250	1250
−35–25	1000	1000	1000	1020	1030	1030	1330	1330	1330	1330	1330	1330
−45–35	970	970	970	1030	1040	1040	1380	1380	1380	1380	1380	1380
−55–45	1060	1060	1060	1070	1080	1080	1420	1420	1420	1420	1420	1420
−65–55	1100	1100	1100	1100	1100	1100	1430	1430	1430	1430	1430	1430
Lat	Winter: night-time						Winter: day-time					
55–65	910	910	910	910	910	910	1363	1363	1363	1363	1363	1363
45–55	880	900	900	908	916	917	1293	1293	1293	1293	1293	1293
35–45	721	729	731	736	736	738	1224	1224	1224	1224	1224	1224
25–35	672	679	682	685	685	689	1200	1200	1200	1200	1200	1200
15–25	667	660	660	653	653	660	1190	1190	1190	1190	1190	1190
5–15	687	680	680	680	680	680	1170	1170	1170	1170	1170	1170
0	1000	1000	1000	1000	1000	1000	1150	1150	1150	1150	1150	1150
−15–5	1028	978	948	948	948	948	1170	1170	1170	1170	1170	1170
−25–15	686	686	686	726	766	726	1180	1180	1180	1180	1180	1180
−35–25	660	660	660	695	730	690	1200	1200	1200	1200	1200	1200
−45–35	731	731	731	811	881	811	1220	1220	1220	1220	1220	1220
−55–45	998	898	848	938	998	998	1293	1293	1293	1293	1293	1293
−65–55	1100	1100	1100	1100	1100	1100	1363	1363	1363	1363	1363	1363

Values sorted according to geomagnetic latitude and longitude.

season, local time, longitude and latitude. The model has been recently upgraded (Stankov, 2002a; Stankov et al., 2003a) to provide better diurnal and longitudinal variations at low solar activity conditions. Other models also exist and can be implemented as well (Marinov et al., 2004).

6. Results and discussion

The reconstruction method has been tested extensively for various spatial and temporal conditions. Several aspects of this reconstruction have been considered, e.g., what effects will input parameter changes have on the reconstruction results; which ionospheric profiler will be better suited for a given location, time and ionosphere–plasmasphere status; qualitative and quantitative analysis of the reconstructed density profiles including comparison with empirical models; possible applications, opportunities for improvement, etc. All required TEC values have been obtained from CHAMP observations using GPS.

6.1. Exemplary calculations using CHAMP measurements

At first, reconstruction tests have been performed with the Sech-squared profiler after finding coincidences between the CHAMP and ionosonde measurements. Normally, there is a great number of such coincidences in the European region considering the good coverage provided by the satellite and the high density of ionosonde stations.

As an example, presented are the reconstructed topside oxygen and hydrogen ion density profiles together with the corresponding full-height electron profile (Fig. 3). Notice that for altitudes above h_mF_2 the electron density at a given height is obtained after summing up the corresponding ion densities. It is therefore assumed that the principle of plasma quasi-neutrality holds true. In the given example, selected is the site of the North-European ionosonde station Juliusruh (JR055: 54.63°N, 13.38°E) on 14/03/2001 for night-time conditions (03:18UT) and on 16/03/2001 for day-time conditions (15:41UT). At this latitude, the effect of the vertical

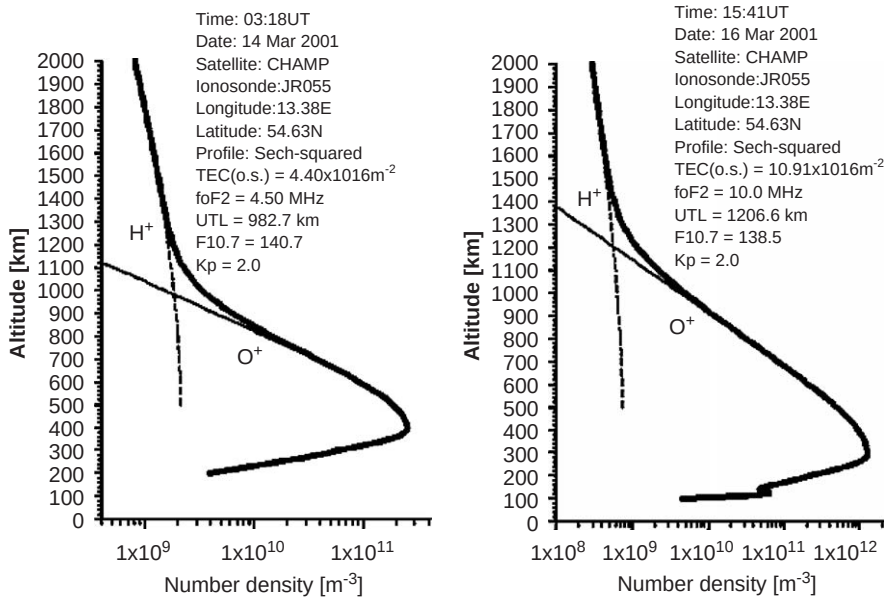

Fig. 3. Reconstructed ion and electron density profiles at the site of the Juliusruh ionosonde station (JR055: 54.63°N, 13.38°E) for night-time and day-time conditions. The topside part of the electron profile is obtained after summing up the O^+ and H^+ ion densities.

correction factor is relatively small. The selected days are typical near-equinox days with quiet geomagnetic activity ($K_p = 2.00$) and relatively high solar activity conditions ($F_{10.7} = 140.7$[W/m^2/Hz], 138.5[W/m^2/Hz]). The required input parameters are as follows: over-satellite electron content ($sTEC = 4.40 \times 10^{16}$[m^{-2}], 10.91×10^{16}[m^{-2}]), height of satellite ($h_s = 419.5$[km], 423.2[km]), upper transition level ($h_{tr} = 982.7$[km], 1206.6[km]), F_2-layer critical frequency ($f_oF_2 =$ 4.5[MHz], 10.0[MHz]), E-layer critical frequency ($f_oE = 0.0$[MHz], 2.3[MHz]), and propagation factor ($M_{3000}F_2 = 2.6$, 3.1). The calculated O^+ scale height is about 93.3 km for the night-time profile and slightly higher—about 100.3 km—for the day-time profile. Such an increase is a consequence of the complex interplay of the three major shape factors for the top-side profile—on the one hand, increased O^+ peak density (from about 2.5×10^{11} m^{-3} at night to about 1.2×10^{12} m^{-3} at day), but on the other hand, decreased peak density height (from 396.7 km at night to 294.5 km at day) and increased ion transition level (from 982.7 km at night up to 1206.6 km at day). A greater difference is observed between the calculated night-time and day-time H^+ ion scale heights.

The reconstruction method provides a good opportunity to estimate the contribution of the upper ionosphere and/or the plasmasphere into the total electron content. In the above example, the night-time TEC_{total} is estimated at 6.75 TECU with TEC_{top} of 4.97 TECU, hence the combined upper ionosphere and plasmasphere contribution of about 73.6% from the total. In the day-time case, TEC_{total} is estimated at 32.85 TECU with TEC_{top} of 24.99 TECU, hence a combined contribution of about 76.1% from the total. Considering the availability of concurrent information about the bottom-side ionosphere (through the ionosonde), all this can lead to a better understanding of the ionosphere–plasmasphere system's status, ionization, coupling, and other processes.

6.2. Vertical correction factor—conditions and effects

As mentioned before (Section 2), the plasma transport occurs predominantly along the geomagnetic field line while we are interested in obtaining the density distribution in vertical direction. The discrepancy is negligible at high geomagnetic latitudes, but at lower and equatorial latitudes the tilt of the geomagnetic field lines (dip) should be of concern.

It follows from simple geometrical considerations (Fig. 2) that $\mathbf{dh} = \sin I\,\mathbf{ds}$, where **dh**—differential element along the vertical axis, **ds**—differential element along the field line. This relationship is applied to the ion scale heights instead of the densities in order to avoid the usual practice of performing calculations along several field lines. Common sources for the inclination are measurements at a given observing station or model values derived from a spherical harmonics expansion of the geomagnetic field. Sometimes the inclination in the ionosphere (e.g. at the F_2 peak height, h_mF_2) is taken instead of the inclination at the ground. The construction here simply adopts the relation between magnetic latitude and inclination (dip angle) for a dipole leading to the equation $\tan\varphi = 0.5\tan I$ (where φ is the dip latitude, I is the inclination). Finally, the correction factor is found to be: $\xi = \sin[\arctan(2.\tan\varphi)]$. In effect,

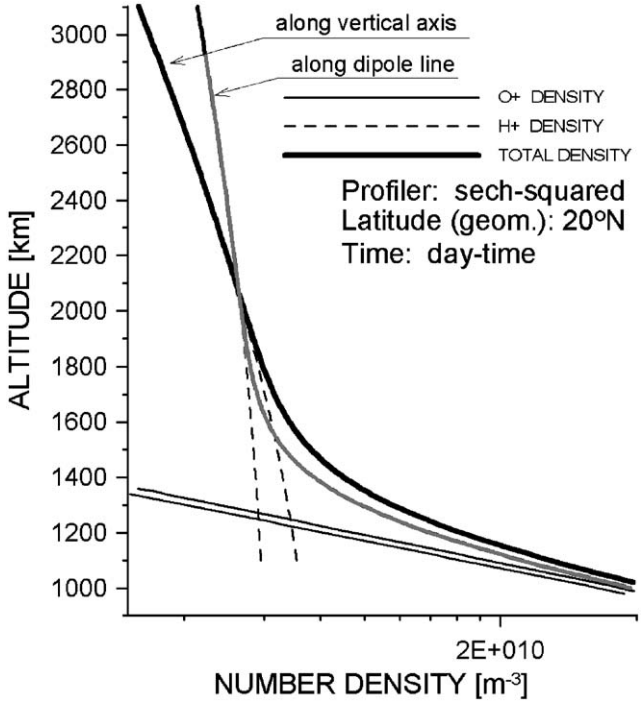

Fig. 4. Density profiling along the dipole field line and vertical axis.

the use of the factor leads to a redistribution of the plasma density in height direction as demonstrated for the geomagnetic latitude of 20.0°N (Fig. 4). The difference between the two types of profiling—the one along the dipole field line and the other along the vertical axis is clearly visible in the figure. While there is no much difference between the electron profiles in the topside ionosphere, the discrepancies become obvious near the UTL and above in the plasmasphere, where the profile along the field line is much steeper than the vertical profile.

In conclusion, the technique offered in this paper is supposed to be used at middle and high geomagnetic latitudes. Covering the equatorial region would require additional developments related to complex local phenomena such as the $E \times B$ drift and inter-hemispheric flows.

6.3. Selection of ionospheric profiler

The method was originally developed using the Sech-squared profiler. Later on, the use of the Exponential model was studied for reconstruction purposes. Both models produce quite different (in shape) top-side density profiles which is demonstrated (Fig. 5, top panel) for a given scale height of 100 km, maximum density of $1 \times 10^5 [\mathrm{cm}^{-3}]$, and height of the peak density of 300 km. It is also evident that the Sech-squared topside profile tends to asymptotically approach the exponential profile at very great altitudes ($h \gg h_m F_2$).

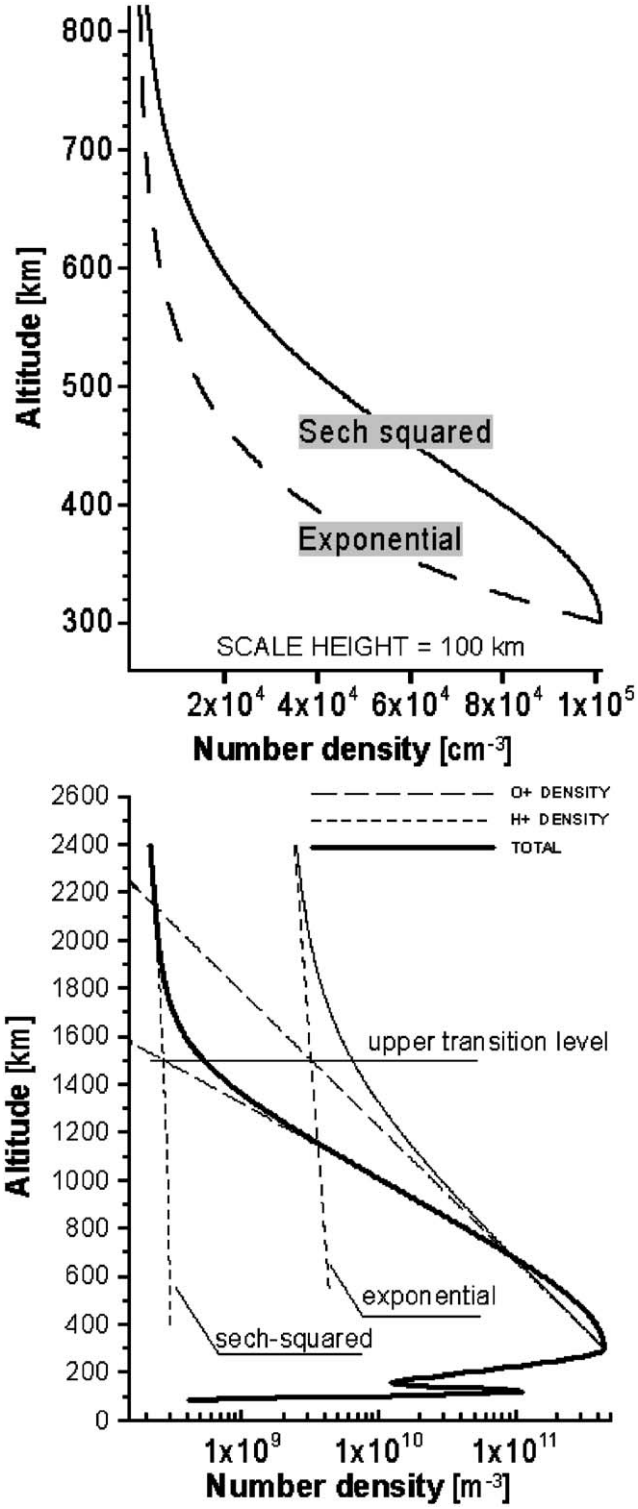

Fig. 5. Comparison between profile reconstructions based on Sech-squared and Exponential models for fixed values of TEC and UTL.

The demonstrated large differences in the profile shapes proves once again the necessity of an 'anchor' somewhere above $h_m F_2$ which would point at the most appropriate model. As written before, the UTL value can successfully play this role. In fact, the information

about the UTL is not used outside the solution but is rather introduced into the equation about the O^+ scale height which is the better approach. It is obvious from the vertical density distribution produced with a same scale height for all profilers that larger density values at all altitudes are obtained with the Sech-squared profiler and smaller—with the Exponential profiler. Hence, for a fixed scale height, larger TEC values are expected from the Sech-squared profiler and smaller—from the Exponential profiler. From a reconstruction point of view however, we need to investigate how the reconstructed profiles will behave when forced to satisfy the UTL conditions for a fixed TEC and UTL values. In order to preserve the same TEC value, the O^+ scale height calculated using the reconstructed method should be larger if the Exponential model is employed, and oppositely, it should be smaller if the Sech-squared model is used. To prove that, electron profiles were deduced using fixed TEC of $34.9 \times 10^{16} m^{-2}$ and UTL of 1400 km (Fig. 5, bottom panel). As expected, the scale heights obtained via the Exponential profiler are higher, thus yielding much steeper electron density profile. As a result of the differences in the calculated oxygen ion scale heights, significant differences are observed in the hydrogen ion density profiles—both in scale height and in absolute ion density values. The increased ion scale height obtained via the Exponential profiler leads to higher electron density at greater altitudes and therefore higher contribution to TEC from the plasmasphere, which should be expected during daytime.

The way in which the plasma diffusion controls the F layer has been well investigated during the years. During the night, the F layer develops into a stationary (but decaying) form resembling a Chapman layer. During the day, the electron density near the F_2 peak approximates to the equilibrium value which it would have in the absence of diffusion. Above the peak the electron density is mainly controlled by plasma diffusion and at greater altitudes the distribution is expected to be exponential with a scale height corresponding to the mass of the positive ions. The variation of electron density is then largely controlled by the variation of the peak electron density N_mF_2 which is a key input parameter in the proposed reconstruction technique and is provided—with a high precision—by ground ionosonde(s). By using ground-based TEC measurements, it has been confirmed that the vertical distribution of the major ion can be successfully reconstructed with the exponential profiler under some conditions but particularly for the day-time ionosphere (Stankov, 2002c).

6.4. Comparison with IRI calculations

From previous studies (Belehaki et al., 2004a, b) with ground digisonde reconstructions (Reinisch, 1996; Huang and Reinisch, 2001) it has been found that the latter tend to underestimate the contribution from the plasmasphere, thus the topside electron profiles are strongly depleted. The reason is probably in the use of the Chapman profiler for deducing the top-side ionosonde-based profiles. It has been estimated that ITEC (the ground ionosonde derived TEC value) is generally within ~10% of the GPS TEC and also that the Chapman profile above 700 km contributes less than ~2% of the total content. Since a large portion of the TEC is delivered by the electron profile immediately above the F_2 peak height, the correct determination of the plasma scale height in this region is of utmost importance.

As a step in the evaluation of the described reconstruction method, here we compare representative reconstruction results with corresponding electron profiles deduced from IRI (Bilitza et al., 1993;Bilitza, 2001) model calculations. For this purpose, several CHAMP observations of TEC have been selected for the site of the Juliusruh digisonde (54.63°N, 13.38°E) for both night-time (Fig. 6, left panels) and day-time (Fig. 6, right panels) hours, and for summer, equinox, and winter seasons during high solar activity and quiet geomagnetic conditions (Table 3). In order to better compare the topside profiling, the IRI-2001 model has been run in two modes—one, with N_mF_2 and h_mF_2 provided by the model itself (denoted with 'IRI') and another, with N_mF_2 and h_mF_2 provided by the ionosonde measurements (denoted with 'IRI^{adj}').

Below h_mF_2, the electron profiles are calculated similarly, so there are no large discrepancies between the bottom-side sections of the profiles and hence between their electron content values. This fact justifies the more important comparison of the top-side profiles. The IRI simulates the F_2 layer peak density and peak height values well only for the daytime winter and equinox conditions. This underlines the significance of binding our reconstruction method to a reliable source such as the ground ionosonde.

In contrast to the bottom-side ionosphere, above h_mF_2 the differences between the electron profiles of the presented approaches are becoming quite significant. In some cases, there is a good agreement between topside scale heights obtained from IRI and the Over-Satellite Electron Content (OSEC) reconstruction method, particularly during summer. However, in the rest of the cases, large differences are observed. A possible reason can be the climatological features in IRI, but also, inaccuracies in the ion transition level values. The importance of the ion transition level in reconstructing the topside density distribution has been already pointed out. The results here also confirm the necessity of this additional information to be included in the reconstruction. IRI profiles show constant transition levels which is not realistic (Kutiev et al., 1980; Stankov, 2002a). One

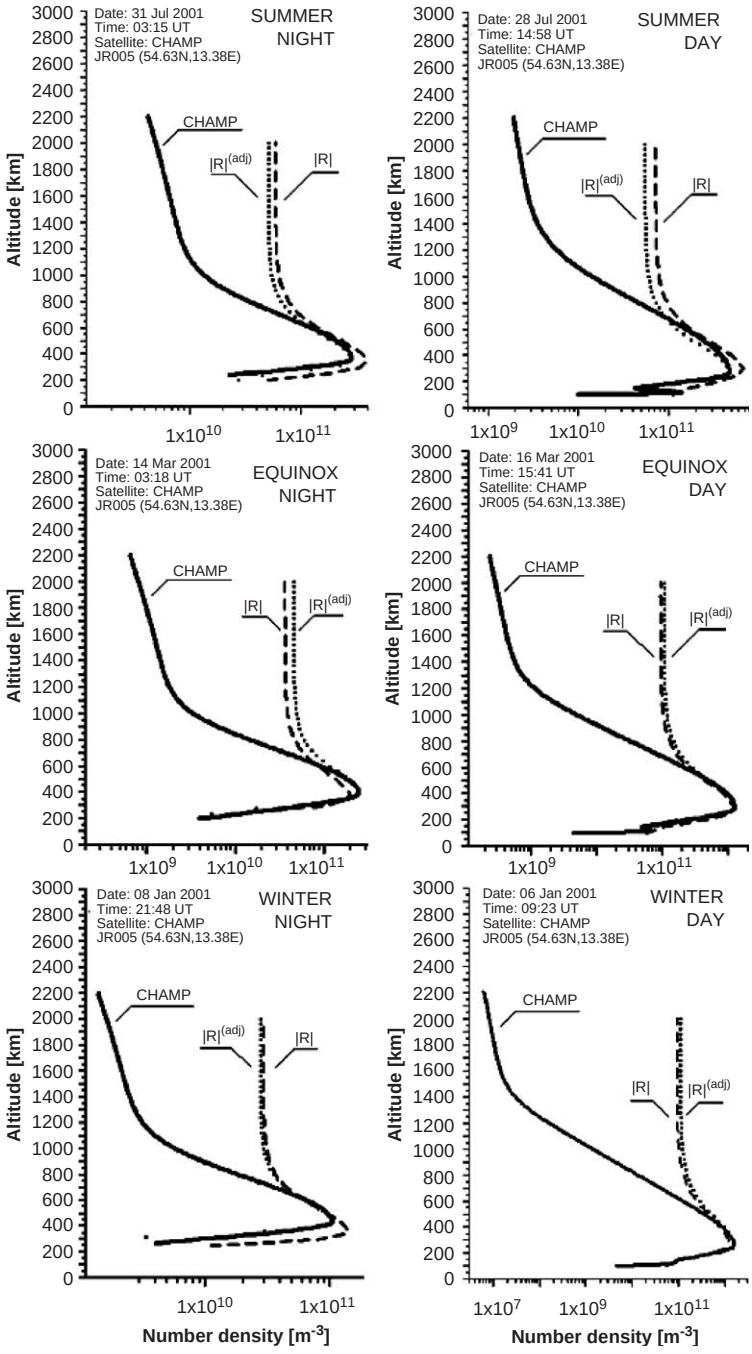

Fig. 6. Reconstructed electron profiles (solid line) using CHAMP OSEC compared with the corresponding profiles calculated from IRI-2001 (dashes) and IRI-2001 adjusted to the peak density characteristics (dots). Left panels: night-time conditions, right panels: day-time conditions.

significant consequence is the overestimated electron density in the plasmasphere. Evidences of some discrepancies between measured and IRI-modelled top-side electron profiles do exist (Jakowski and Tsybulya, 2004). Considering that we are using UTL model values from independent sources, it is quite possible that the figures really show overestimated plasmasphere profiles from IRI. In addition, the OSEC reconstruction method offers better H^+ scale height, more realistically bound to the current geophysical conditions through its connection to the top-side O^+ scale height, the UTL and TEC measurements.

7. Summary and conclusions

Presented was a new approach to reconstructing the topside ion and electron density distribution from

Table 3
Reconstruction of the electron profiles: required input data and results

Season Parameter	Winter Night	Winter Day	Equinox Night	Equinox Day	Summer Night	Summer Day
Geogr.Coord's	13.4°E,	13.4°E,	13.4°E,	13.4°E,	13.4°E,	13.4°E,
(deg)	54.6°N	54.6°N	54.6°N	54.6°N	54.6°N	54.6°N
Geom.Coord's	99.7°E,	99.7°E,	99.7°E,	99.7°E,	99.7°E,	99.7°E,
(deg)	54.3°N	54.3°N	54.3°N	54.3°N	54.3°N	54.3°N
Date	08.01.2001	06.01.2001	14.03.2001	16.03.2001	31.07.2001	28.07.2001
DoY	8	6	73	75	212	209
UT (h)	21:48	09:22	03:18	15:41	03:15	14:58
LT (h)	22:48	10:22	04:18	16:41	04:15	15:58
F10.7 ($W/m^2/Hz$)	161.5	173.4	140.7	138.5	120.3	119.0
K_p	2.33	1.00	2.00	2.00	4.00	2.00
EC_{OS} (m^{-2})	2.90×10^{16}	4.98×10^{16}	4.40×10^{16}	10.91×10^{16}	5.83×10^{16}	6.30×10^{16}
EC_{TOT} (m^{-2})	3.64×10^{16}	35.85×10^{16}	6.75×10^{16}	32.85×10^{16}	10.10×10^{16}	17.45×10^{16}
f_oF_2 (MHz)	2.90	11.20	4.50	10.00	4.80	6.20
f_oE (MHz)	0.00	2.25	0.00	2.25	0.00	3.35
$M_{3000}F_2$	2.40	3.35	2.55	3.05	2.70	2.90
N_mF_2 (m^{-3})	1.042×10^{11}	1.555×10^{12}	2.511×10^{11}	1.239×10^{12}	2.857×10^{11}	4.767×10^{11}
H_mF_2 (km)	433.90	258.02	396.73	294.48	364.69	269.02
H_{LEO} (km)	433.95	461.27	419.51	423.17	453.66	460.23
UTL (km)	1001.42	1401.87	982.73	1206.59	917.34	1176.59
H_{O+} (km)	114.90	88.18	93.33	100.33	115.96	141.89

The ionosonde measurements are made at Juliusruh, JR055 (54.63N, 13.38E).

space-based observations of the total electron content and concurrent ground-based ionosonde measurements. The method utilizes additional information on the oxygen–hydrogen ion transition level in order to uniquely determine the unknown ion scale heights. As a result, ion and electron density profiles are reconstructed and bound to the observed geophysical conditions.

The efficiency of a reconstruction method should be considered from several aspects including reliability, availability of measurements, and applicability of results. The reliability of the approach is based on previously developed reconstruction techniques for ground based observations—both TEC and ionosonde. Also, the method employs precise and efficient numerical methods. During the years the LEO satellites have been providing observations in abundance and with good temporal and spatial coverage. The availability of TEC measurements is guaranteed by current (CHAMP, SAC-C, GRACE) and future (e.g. COSMIC—Constellation Observing System for Meteorology Ionosphere and Climate) LEO missions.

The here presented reconstruction method has been tested on actual measurements from the CHAMP satellite and the following conclusions can be made:

- The method tightens the density profiles to existing ground and space based observations, thus ensuring higher reliability.
- The technique can complement the digisonde profile reconstruction to yield better results for the top-side ionosphere and the plasmasphere.
- The IRI model tends to generally overestimate the topside ionospheric and plasmaspheric contribution.
- The LEO satellite fleet, together with the advanced global navigation satellite systems, offer rich opportunities.

Several important applications are envisaged. Current and future LEO satellite missions, together with the development of complex global navigation satellite systems, offer opportunities to apply the proposed reconstruction technique in ionosphere–plasmasphere system monitoring (Stankov et al., 2003b), in evaluating and improving empirical and theoretical ionosphere–plasmasphere models, in better studying the ion composition, ionosphere–plasmasphere coupling, ionospheric irregularities, etc.

Acknowledgements

The authors thank Dr. P. Muhtarov and Dr. I. Kutiev for the useful discussions. Thanks are also due to the members of the CHAMP teams in DLR and GFZ for the high-quality data acquisition and processing. This research has been funded by the German Aerospace Centre, the German State Government of Mecklenburg-Vorpommern under Grant V230-630-08-TIFA-334, and by the NATO Science Program under Grants EST.CLG.977103 and EST.CLG.979784.

References

Austen, J.R., Franke, S.J., Liu, C.H., 1988. Ionospheric imaging using computerized tomography. Radio Sci. 23, 299–307.

Belehaki, A., Jakowski, N., Reinisch, B.W., 2004a. Plasmaspheric electron content derived from GPS TEC and digisonde ionograms. Adv. Space Res. 33 (6), 833–837.

Belehaki, A., Jakowski, N., Reinisch, B.W., 2004b. Comparison of ionospheric ionisation measurements over Athens using ground ionosonde and GPS derived TEC values. Radio Sci. 38 (6), 1105.

Bilitza, D., 2001. International Reference Ionosphere 2000. Radio Sci. 36 (2), 261–275.

Bilitza, D., Rawer, K., 1996. International Reference Ionosphere. In: Dieminger, W., Hartmann, G.K., Leitinger, R. (Eds.), The Upper Atmosphere—Data Analysis and Interpretation. Springer, Berlin, pp. 735–772.

Bilitza, D., Rawer, K., Bossy, L., Gulyaeva, T., 1993. International Reference Ionosphere—past, present and future: II. Plasma temperatures, ion composition and ion drift. Adv. Space Res. 13 (3), 15–23.

Coco, D., 1991. GPS—satellites of opportunity for ionospheric monitoring. GPS World, October 1991, pp. 47–50.

Daniell, R.E., Brown, L.D., Anderson, D.N., Fox, M.W., Doherty, P.H., Decker, D.T., Sojka, J.J., Schunk, R.W., 1995. Parameterized ionospheric model: a global ionospheric parameterization based on first principles models. Radio Sci. 30, 1499–1510.

Davies, K., 1990. Ionospheric Radio. Peter Peregrinus Ltd., London, UK.

Davies, K., 1996. Ionosphere models. In: Dieminger, W., Hartmann, G.K., Leitinger, R. (Eds.), The Upper Atmosphere—Data Analysis and Interpretation. Springer, Berlin, pp. 693–705.

Davies, K., Hartmann, G.K., 1997. Studying the ionosphere with the global positioning system. Radio Sci. 84, 1695–1703.

Di Giovanni, G., Radicella, S.M., 1990. An analytical model of the electron density profile in the ionosphere. Adv. Space Res. 10 (11), 27–30.

Dudeney, J.R., 1983. The accuracy of simple methods for determining the height of the maximum electron concentration of the F_2-layer from scaled ionospheric characteristics. J. Atmos. Terr. Phys. 45 (8/9), 629–640.

Fjeldbo, G.F., Eshleman, V.R., Kliore, A.J., 1971. The neutral atmosphere of Venus as studied with the Mariner V radio occultation experiments. Astron. J. 76, 123–140.

Gurvich, A.S., Krasilnikova, T.G., 1990. Navigation satellites for radio sensing of the Earth's atmosphere. Soviet J. Remote Sensing 7, 1124–1131.

Heise, S., Jakowski, N., Wehrenpfennig, A., Reigber, C., Luehr, H., 2002. Sounding of the topside ionosphere/plasmasphere based on GPS measurements from CHAMP: initial results. Geophys. Res. Lett. 29, 14.

Hoeg, P., Hauchecorne, A., Kirchengast, G., Syndergaard, S., Belloul, B., Leitinger, R., Rothleitner, W., 1995. In: Hoeg, P., Syndergaard, S. (Eds.), Derivation of Atmospheric Properties Using a Radio Occultation Technique. ESA/ESTEC Contract Report 11024/94/NL/CN, DMI Scientific Report 95-4. Danish Meteorological Institute, Copenhagen.

Huang, X., Reinisch, B.W., 1982. Automatic calculation of electron density profiles from digital ionograms: 2. True height inversion of topside ionograms with the profile-fitting method. Radio Sci. 17 (4), 837–844.

Huang, X., Reinisch, B.W., 2001. Vertical electron content from ionograms in real time. Radio Sci. 36 (2), 335–342.

Jakowski, N., 1996. TEC monitoring by using satellite positioning systems. In: Kohl, H., Ruester, R., Schlegel, K. (Eds.), Modern Ionospheric Science. European Geophysical Society, Katlenburg-Lindau, pp. 371–390.

Jakowski, N., Tsybulya, K., 2004. Comparison of ionospheric radio occultation CHAMP data with IRI2001. Adv. Radio Sci. 2, 275–279.

Jakowski, N., Wehrenpfennig, A., Heise, S., Reigber, C., Luehr, H., Grunwaldt, L., Meehan, T.K., 2002. GPS radio occultation measurements of the ionosphere from CHAMP: early results. Geophys. Res. Lett. 29, 10.

Kutiev, I., Heelis, R.A., Sanatani, S., 1980. The behaviour of the O^+–H^+ transition level at solar maximum. J. Geophys. Res. 85 (A5), 2366–2371.

Kutiev, I., Stankov, S.M., Marinov, P., 1994. Analytical expression of O^+–H^+ transition surface for use in IRI. Adv. Space Res. 14 (12), 135–138.

Leitinger, R., 1996a. Ionospheric electron content. In: Dieminger, W., Hartmann, G.K., Leitinger, R. (Eds.), The Upper Atmosphere—Data Analysis and Interpretation. Springer, Berlin, pp. 660–672.

Leitinger, R., 1996b. Tomography. In: Kohl, H., Ruester, R., Schlegel, K. (Eds.), Modern Ionospheric Science. European Geophysical Society, Katlenburg-Lindau, pp. 346–370.

Marinov, P., Kutiev, I., Watanabe, S., 2004. Empirical model of O^+–H^+ transition height based on topside sounder data. Adv. Space Res. 34, 2021–2025.

Rawer, K., 1988. Synthesis of ionospheric electron density profiles with Epstein functions. Adv. Space Res. 8 (4), 191–198.

Reigber, C., Luehr, H., Schwintzer, P., 2003. First CHAMP Mission Results for Gravity, Magnetic and Atmospheric Studies. Springer, Berlin.

Reinisch, B.W., 1996. Modern ionosondes. In: Kohl, H., Ruester, R., Schlegel, K. (Eds.), Modern Ionospheric Science. European Geophysical Society, Katlenburg-Lindau, pp. 440–458.

Reinisch, B.W., Huang, X., 1982. Automatic calculation of electron density profiles from digital ionograms: 1. Automatic O and X trace identification for topside ionograms. Radio Sci. 17 (2), 421–434.

Reinisch, B.W., Huang, X., 1983. Automatic calculation of electron density profiles from digital ionograms: 3. Processing of bottomside ionograms. Radio Sci. 18 (3), 477–492.

Reinisch, B.W., Haines, D.M., Benson, R.F., Green, J.L., Sales, G.S., Taylor, W.W.L., 2001. Radio sounding in space: magnetosphere and topside ionosphere. J. Atmos. Sol.-Terr. Phys. 63, 87–98.

Stankov, S.M., 2002a. Empirical modelling of ion transition levels based on satellite in situ measurements. C. R. Acad. Bulg. Sci. 55 (1), 35–40.

Stankov, S.M., 2002b. Reconstruction of the upper electron density profile from the over-satellite electron content. C. R. Acad. Bulg. Sci. 55 (2), 31–36.

Stankov, S.M., 2002c. Evaluation of theoretical profilers used in the electron density profile reconstruction. Acta Geodaetica Geophys. Hung. 37 (4), 385–401.

Stankov, S.M., Muhtarov, P.Y., 2001. Reconstruction of the electron density profile from the total electron content using upper transition level and vertical incidence sounding measurements. C. R. Acad. Bulg. Sci. 54 (9), 45–48.

Stankov, S.M., Kutiev, I.S., Jakowski, N., Heise, S., 2002. Electron density profiles deduced from GPS TEC, O^+–H^+ transition height and ionosonde data. Acta Geodaetica Geophys. Hung. 37 (2–3), 171–181.

Stankov, S.M., Jakowski, N., Heise, S., Muhtarov, P., Kutiev, I., Warnant, R., 2003a. A new method for reconstruction of the vertical electron density distribution in the upper ionosphere and plasmasphere. J. Geophys. Res. 108 (A5), 1164.

Stankov, S.M., Warnant, R., Jodogne, J.C., 2003b. Real-time reconstruction of the vertical electron density distribution from GPS-TEC measurements. Acta Geodaetica Geophys. Hung. 38 (4), 377–388.